First Search for $B \to X_s \nu\bar{\nu}$ Decays

M. Abumusabh, I. Adachi, K. Adamczyk, L. Aggarwal, H. Ahmed, Y. Ahn, H. Aihara, N. Akopov, S. Alghamdi, M. Alhakami, A. Aloisio, N. Althubiti, K. Amos, N. Anh Ky, C. Antonioli, D. M. Asner, H. Atmacan, T. Aushev, M. Aversano, R. Ayad, V. Babu, H. Bae, N. K. Baghel, S. Bahinipati, P. Bambade, Sw. Banerjee, M. Barrett, M. Bartl, J. Baudot, A. Baur, A. Beaubien, F. Becherer, J. Becker, J. V. Bennett, F. U. Bernlochner, V. Bertacchi, M. Bertemes, E. Bertholet, M. Bessner, S. Bettarini, V. Bhardwaj, B. Bhuyan, F. Bianchi, T. Bilka, D. Biswas, A. Bobrov, D. Bodrov, A. Bondar, G. Bonvicini, J. Borah, A. Boschetti, A. Bozek, M. Bračko, P. Branchini, R. A. Briere, T. E. Browder, A. Budano, S. Bussino, Q. Campagna, M. Campajola, L. Cao, G. Casarosa, C. Cecchi, M.-C. Chang, P. Chang, P. Cheema, L. Chen, B. G. Cheon, C. Cheshta, H. Chetri, K. Chilikin, J. Chin, K. Chirapatpimol, H.-E. Cho, K. Cho, S.-J. Cho, S.-K. Choi, S. Choudhury, J. A. Colorado-Caicedo, I. Consigny, L. Corona, J. X. Cui, E. De La Cruz-Burelo, S. A. De La Motte, G. de Marino, G. De Nardo, G. De Pietro, R. de Sangro, M. Destefanis, S. Dey, A. Di Canto, J. Dingfelder, Z. Doležal, I. Domínguez Jiménez, T. V. Dong, X. Dong, K. Dugic, G. Dujany, P. Ecker, R. Farkas, P. Feichtinger, T. Ferber, T. Fillinger, C. Finck, G. Finocchiaro, F. Forti, A. Frey, B. G. Fulsom, A. Gabrielli, A. Gale, E. Ganiev, M. Garcia-Hernandez, R. Garg, L. Gärtner, G. Gaudino, V. Gaur, V. Gautam, A. Gaz, A. Gellrich, G. Ghevondyan, D. Ghosh, H. Ghumaryan, G. Giakoustidis, R. Giordano, A. Giri, P. Gironella Gironell, A. Glazov, B. Gobbo, R. Godang, O. Gogota, P. Goldenzweig, W. Gradl, E. Graziani, D. Greenwald, Y. Guan, K. Gudkova, I. Haide, Y. Han, C. Harris, H. Hayashii, S. Hazra, C. Hearty, M. T. Hedges, A. Heidelbach, G. Heine, I. Heredia de la Cruz, M. Hernández Villanueva, T. Higuchi, M. Hoek, M. Hohmann, R. Hoppe, P. Horak, X. T. Hou, C.-L. Hsu, A. Huang, T. Humair, T. Iijima, K. Inami, G. Inguglia, N. Ipsita, A. Ishikawa, R. Itoh, M. Iwasaki, P. Jackson, D. Jacobi, W. W. Jacobs, D. E. Jaffe, E.-J. Jang, Q. P. Ji, S. Jia, Y. Jin, A. Johnson, K. K. Joo, A. B. Kaliyar, J. Kandra, K. H. Kang, S. Kang, G. Karyan, T. Kawasaki, F. Keil, C. Ketter, C. Kiesling, C.-H. Kim, D. Y. Kim, J.-Y. Kim, K.-H. Kim, Y.-K. Kim, H. Kindo, K. Kinoshita, P. Kodyš, T. Koga, S. Kohani, K. Kojima, A. Korobov, S. Korpar, E. Kovalenko, R. Kowalewski, P. Križan, P. Krokovny, T. Kuhr, Y. Kulii, D. Kumar, K. Kumara, T. Kunigo, A. Kuzmin, Y.-J. Kwon, S. Lacaprara, K. Lalwani, T. Lam, J. S. Lange, T. S. Lau, M. Laurenza, R. Leboucher, F. R. Le Diberder, H. Lee, M. J. Lee, C. Lemettais, P. Leo, P. M. Lewis, C. Li, H.-J. Li, L. K. Li, Q. M. Li, S. X. Li, W. Z. Li, Y. Li, Y. B. Li, Y. P. Liao, J. Libby, J. Lin, S. Lin, Z. Liptak, M. H. Liu, Q. Y. Liu, Y. Liu, Z. Liu, D. Liventsev, S. Longo, A. Lozar, T. Lueck, T. Luo, C. Lyu, J. L. Ma, Y. Ma, M. Maggiora, S. P. Maharana, R. Maiti, G. Mancinelli, R. Manfredi, E. Manoni, M. Mantovano, D. Marcantonio, S. Marcello, C. Marinas, C. Martellini, A. Martens, T. Martinov, L. Massaccesi, M. Masuda, D. Matvienko, S. K. Maurya, M. Maushart, J. A. McKenna, Z. Mediankin Gruberová, R. Mehta, F. Meier, D. Meleshko, M. Merola, C. Miller, M. Mirra, S. Mitra, K. Miyabayashi, H. Miyake, R. Mizuk, G. B. Mohanty, S. Mondal, S. Moneta, A. L. Moreira de Carvalho, H.-G. Moser, M. Mrvar, H. Murakami, R. Mussa, I. Nakamura, M. Nakao, Y. Nakazawa, M. Naruki, Z. Natkaniec, A. Natochii, M. Nayak, M. Neu, S. Nishida, R. Nomaru, S. Ogawa, R. Okubo, H. Ono, Y. Onuki, F. Otani, G. Pakhlova, A. Panta, S. Pardi, K. Parham, J. Park, S.-H. Park, B. Paschen, A. Passeri, S. Patra, S. Paul, T. K. Pedlar, I. Peruzzi, R. Pestotnik, M. Piccolo, L. E. Piilonen, P. L. M. Podesta-Lerma, T. Podobnik, C. Praz, S. Prell, E. Prencipe, M. T. Prim, S. Privalov, I. Prudiiev, H. Purwar, P. Rados, G. Raeuber, S. Raiz, V. Raj, K. Ravindran, J. U. Rehman, M. Reif, S. Reiter, L. Reuter, D. Ricalde Herrmann, I. Ripp-Baudot, G. Rizzo, S. H. Robertson, J. M. Roney, A. Rostomyan, N. Rout, L. Salutari, D. A. Sanders, S. Sandilya, L. Santelj, C. Santos, V. Savinov, B. Scavino, C. Schmitt, S. Schneider, M. Schnepf, K. Schoenning, C. Schwanda, Y. Seino, A. Selce, K. Senyo, J. Serrano, M. E. Sevior, C. Sfienti, W. Shan, G. Sharma, X. D. Shi, T. Shillington, T. Shimasaki, J.-G. Shiu, D. Shtol, B. Shwartz, A. Sibidanov, F. Simon, J. B. Singh, J. Skorupa, R. J. Sobie, M. Sobotzik, A. Soffer, A. Sokolov, E. Solovieva, S. Spataro, K. Špenko, B. Spruck, M. Starič, P. Stavroulakis, S. Stefkova, R. Stroili, M. Sumihama, K. Sumisawa, N. Suwonjandee, H. Svidras, M. Takahashi, M. Takizawa, U. Tamponi, S. Tanaka, S. S. Tang, K. Tanida, F. Tenchini, F. Testa, A. Thaller, T. Tien Manh, O. Tittel, R. Tiwary, E. Torassa, F. F. Trantou, I. Tsaklidis, M. Uchida,

I. Ueda, T. Uglov, K. Unger, Y. Unno, K. Uno, S. Uno, P. Urquijo, Y. Ushiroda, S. E. Vahsen, R. van Tonder, K. E. Varvell, M. Veronesi, V. S. Vismaya, L. Vitale, V. Vobbilisetti, R. Volpe, M. Wakai, S. Wallner, M.-Z. Wang, X. L. Wang, Z. Wang, A. Warburton, S. Watanuki, C. Wessel, E. Won, X. P. Xu, S. Yamada, W. Yan, S. B. Yang, J. Yelton, K. Yi, J. H. Yin, K. Yoshihara, C. Z. Yuan, J. Yuan, L. Zani, F. Zeng, M. Zeyrek, B. Zhang, V. Zhilich, J. S. Zhou, Q. D. Zhou, L. Zhu, and R. Žlebčík

(The Belle II Collaboration)

(Received 17 November 2025; revised 12 February 2026; accepted 11 March 2026; published 10 June 2026)

We report the first search for the flavor-changing neutral-current decays $B \to X_s \nu\bar{\nu}$, where X_s is a hadronic system with strangeness equal to 1, in data collected with the Belle II detector at the SuperKEKB asymmetric-energy e^+e^- collider. The data sample corresponds to an integrated luminosity of 365 fb^{-1} collected at the $\Upsilon(4S)$ resonance and 43 fb^{-1} collected at a center-of-mass energy 60 MeV below resonance for estimation of $e^+e^- \to q\bar{q}$ continuum background. One of the B mesons from the $\Upsilon(4S) \to B\bar{B}$ decay is fully reconstructed in a hadronic decay mode. The $B \to X_s \nu\bar{\nu}$ decay is reconstructed with a sum-of-exclusives approach that uses 30 X_s decay modes. This approach provides high sensitivity to the inclusive decay, despite the presence of two undetected neutrinos. The search is performed in three regions of the X_s mass, $M_{X_s}^{\text{true}}$, chosen to separate contributions from K, $K^*(892)$, and heavier strange final states. We do not observe a significant signal and set upper limits at 90% confidence level on the partial branching fractions for the regions $0.0 < M_{X_s}^{\text{true}} < 0.6$ GeV/c^2, $0.6 < M_{X_s}^{\text{true}} < 1.0$ GeV/c^2, and 1.0 GeV/$c^2 < M_{X_s}^{\text{true}}$ of 2.2×10^{-5}, 9.3×10^{-5}, and 30.9×10^{-5}, respectively. Combining the three mass regions, we obtain the upper limit on the branching fraction, $B(B \to X_s \nu\bar{\nu}) < 3.3 \times 10^{-4}$.

DOI: 10.1103/kf73-hw61

Flavor changing neutral current $b \to s\nu\bar{\nu}$ decays are suppressed in the standard model (SM) due to the GIM mechanism [1], and occur only via loop diagrams (Fig. 1). The absence of charged leptons in the final state allows precise theoretical predictions, in contrast to $b \to s\ell^+\ell^-$ decays, which have contributions from photon exchange between charged particles and a charm loop [2]. The decay rates can be enhanced by physics beyond the SM; for example, virtual contributions from heavy particles such as leptoquarks [3] or a Z' boson [4]. The experimental signature is also sensitive to new invisible particles, such as invisible light scalars [5] or fermionic dark matter [6].

The Belle II collaboration found evidence for the exclusive decay $B^+ \to K^+\nu\bar{\nu}$, measuring a branching fraction $\mathcal{B}(B^+ \to K^+\nu\bar{\nu}) = (2.3 \pm 0.7) \times 10^{-5}$ [7], which is 2.7 standard deviations above the SM prediction, $(5.04 \pm 0.40) \times 10^{-6}$ [8,9]. Inclusive $B \to X_s \nu\bar{\nu}$ decays, where X_s denotes a hadronic system with strangeness equal to 1, have not been studied. The branching fraction $\mathcal{B}(B \to X_s \nu\bar{\nu})$ is predicted to be $(2.9 \pm 0.3) \times 10^{-5}$ in the SM [10], excluding the long-distance contribution from $B^+ \to \tau^+(\to X_s^+\bar{\nu})\nu$ decay. The inclusive $B \to X_s \nu\bar{\nu}$ and exclusive $B \to K\nu\bar{\nu}$ branching fractions have different dependence on the parameters of physics beyond the SM and can be related with a sum rule [6,11], which provides strong motivation for the inclusive search. The ALEPH collaboration searched for b-hadrons decaying with large missing energy at the Z pole and set an upper limit on $\mathcal{B}(b \to s\nu\bar{\nu})$ of 6.4×10^{-4} at 90% confidence level (CL) [12]. However, unlike for B mesons, there is no established theoretical framework that provides reliable predictions for inclusive b-hadron decays.

In this Letter, we report the first search for $B \to X_s \nu\bar{\nu}$, where B and X_s denote both charged and neutral states. The data sample consists of 365.4 ± 1.7 fb^{-1} and contains $(387.1 \pm 5.6) \times 10^6$ $\Upsilon(4S) \to B\bar{B}$ decays collected by the Belle II [13] detector at the SuperKEKB asymmetric-energy e^+e^- collider [14]. An additional sample of 42.7 ± 0.2 fb^{-1} collected at an energy 60 MeV below the $\Upsilon(4S)$ peak (off-resonance data) is used for assessing the

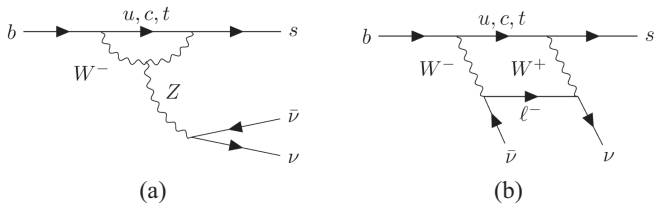


FIG. 1. The leading order SM diagrams for quark-level $b \to s\nu\bar{\nu}$ decays. (a) Penguin diagram. (b) Box diagram.

Published by the American Physical Society under the terms of the Creative Commons Attribution 4.0 International license. Further distribution of this work must maintain attribution to the author(s) and the published article's title, journal citation, and DOI. Funded by SCOAP³.

background from the continuum $e^+e^- \to q\bar{q}$ process, where q is a u, d, s, or c quark.

The Belle II detector consists of a two-layer silicon pixel detector (PXD), a four-layer silicon vertex detector, a central drift chamber (CDC), a time of propagation (TOP) counter, an aerogel ring-imaging Cherenkov detector (ARICH), an electromagnetic calorimeter (ECL), a superconducting solenoid, and a K_L^0 and muon detector (KLM). The symmetry axis of these detectors, defined as the z axis, is approximately in the direction of the electron beam [13].

The Belle II software framework (BASF2) [15,16] is used for event reconstruction. Monte Carlo simulated samples are used to optimize the analysis. B-meson production and decay are simulated using the EvtGen [17] program; $q\bar{q}$ background samples are generated with the Pythia8 [18] and KKMC [19] software; photon radiation from charged particles is simulated using the Photos [20] package; and the Geant4 program is used to simulate the detector response to the passage of particles [21].

We produce signal simulation samples consisting of individually generated contributions: exclusive $B \to K\nu\bar{\nu}$ and $B \to K^*\nu\bar{\nu}$ decays, where K^* denotes the $K^*(892)$ resonance, and nonresonant $B \to X_s\nu\bar{\nu}$ decays. The $B \to K\nu\bar{\nu}$ and $B \to K^*\nu\bar{\nu}$ decays are generated using form factors calculated in lattice QCD computations [8,22] or light-cone sum rules [23]. The nonresonant $B \to X_s\nu\bar{\nu}$ sample is generated with the requirement that the mass $M_{X_s}^{\text{true}}$ of the X_s system be greater than 1.1 GeV/c^2. This requirement is motivated by the study of the $B \to X_s\gamma$ decay [24], as well as $B^0 \to K^+\pi^-\mu^+\mu^-$ and $B^+ \to K^+\pi^+\pi^-\mu^+\mu^-$ decays, which do not show clear components below this mass threshold except K^* resonance [25,26]. The exclusive $K^*\nu\bar{\nu}$ samples are generated without restrictions on the mass $M_{X_s}^{\text{true}}$. To simulate the $M_{X_s}^{\text{true}}$ distribution, we use the Fermi motion model [27–29], assuming the momentum of the b-quark follows a Gaussian distribution. The fragmentation of the final-state hadrons is simulated using Pythia8. The invariant mass squared of the neutrino pair, q^2, is simulated according to the SM [30]. The long-distance $B^+ \to \tau^+(\to X_s^+\bar{\nu})\nu$ decays are treated as background and included in the background sample.

One B meson, denoted B_{tag}, is fully reconstructed in a hadronic decay mode by the full event interpretation (FEI) algorithm [31]. The FEI assigns a probability to each B_{tag} candidate based on a multivariate classifier, indicating how likely the candidate is to be properly reconstructed in a given mode. Candidates with a probability greater than 0.001 are selected. We require B_{tag} candidates to satisfy selections on the beam-energy-constrained mass, $M_{\text{bc}} \equiv \sqrt{(\sqrt{s}/2)^2 - |p_B^* c|^2}/c^2 > 5.27$ GeV/c^2, and the energy difference, $|\Delta E| \equiv |E_B^* - (\sqrt{s}/2)| < 0.2$ GeV. Here, $\sqrt{s}$, p_B^*, and E_B^* are the SuperKEKB center-of-mass (c.m.) energy, and the momentum and energy of the B meson in the c.m. system, respectively.

Particle candidates not used to reconstruct the B_{tag} are used to form the X_s candidate. We use a sum-of-exclusive decays method to reconstruct the X_s candidate, which provides high sensitivity to the inclusive decay, despite the presence of two undetected neutrinos. The X_s candidate is reconstructed in 30 decay modes: $Kn\pi\,(0 \le n \le 4)$ with at most two π^0, and $3Kn\pi\,(0 \le n \le 1)$ with at most one π^0 and one K_S^0, where K indicates $K^\pm$ or K_S^0. These decay modes cover 83% of the nonresonant X_s decay in the signal simulation samples, assuming the K_L^0 contribution is equal to that of K_S^0. In total, the reconstructed modes constitute 93% of the $B \to X_s\nu\bar{\nu}$ branching fraction in the signal simulation samples.

The X_s-candidate reconstruction proceeds as follows. Except for $\pi^\pm$ from K_S^0 candidates, the distance of closest approach of a track to the interaction point (IP) is required to satisfy $dr < 0.5$ cm in the transverse plane and $|dz| < 2$ cm along the z axis. The numbers of hits in the PXD and CDC must be greater than 0 and 20, respectively. Kaon and pion candidates are selected using charged particle identification (PID) likelihoods, built using information from the SVD, CDC, TOP, ARICH, ECL, and KLM subsystems.

Photon candidates are reconstructed from ECL clusters not geometrically matched to charged tracks; to guarantee that clusters do not originate from charged particles, their polar angle θ must be within the CDC acceptance, $17° < \theta < 150°$. The energy of a photon candidate must be greater than 80, 30, or 60 MeV for candidates detected in the forward, barrel, and backward regions of the ECL, respectively.

We reconstruct π^0 candidates from pairs of photon candidates with invariant mass in the range $120 < m_{\gamma\gamma} < 145$ MeV/c^2. The momentum of π^0 candidates must be larger than 0.4 GeV/c. We require the absolute difference in azimuthal angle between the two photons to be less than 1.5 rad in the laboratory frame. Additionally, the opening angle must be smaller than 1.4 rad.

We reconstruct K_S^0 candidates from two oppositely charged tracks, for which a vertex fit [32] is performed and required to converge. The significance of the distance from this vertex to the IP must be larger than 50. We require the invariant mass of K_S^0-candidates to be within 10 MeV/c^2 of the nominal K_S^0 mass [33].

To suppress combinatorial background, the reconstructed invariant mass of the X_s candidate ($M_{X_s}^{\text{reco}}$) must be lower than 2.0 GeV/c^2. A decay-chain vertex fit [32] is required to converge for X_s candidates in decay modes with two or more charged tracks. The c.m.-frame momentum of the X_s must satisfy $0.5 < p_{X_s}^* < 2.96$ GeV/c. To suppress backgrounds from D mesons, X_s candidates with $M_{X_s}^{\text{reco}}$ in the range $[1.84, 1.89]$ GeV/c^2 are rejected. The X_s^0 flavor is assigned based on the net charge of the associated kaons; if

zero, the flavor is undetermined. Pairs of X_s and $B_{\rm tag}$ candidates are further considered only if they have total charge zero and opposite flavor (where determined).

The dineutrino system can be mimicked by particles outside the detector acceptance. Therefore, we require the polar angle of the missing momentum $\vec{p}_{\rm miss} = \vec{p}_{e^+e^-} - \sum \vec{p}_{\rm track} - \sum \vec{p}_{\gamma}$ to be in the detector acceptance, $17° < \theta_{\rm miss} < 150°$. Here, $\vec{p}_{\rm track}$ and $\vec{p}_{\gamma}$ are the momenta of charged tracks and photon candidates.

For each combination of X_s and $B_{\rm tag}$ candidates, the tracks or photon candidates not used in the reconstruction of these candidates form the rest of event. The numbers of tracks from the IP, π^0, and K_S^0 candidates in the rest of event are required to be zero. The rest of event is allowed to contain photon candidates and tracks with $dr > 2$ cm or $|dz| > 4$ cm. We calculate the total lab-frame energy $E_{\rm extra}$ as the sum of all photon candidates with energies greater than 100, 60, and 150 MeV in the forward, barrel, and backward regions of the ECL, respectively. $E_{\rm extra}$ is required to be less than 1.3 GeV, and is further used for background suppression, as explained later.

After these selections, the average multiplicity of $B_{\rm tag}X_s$ candidates per event is 1.71 in simulated signal samples and 1.45 in data. In each event, we retain only the candidates with the highest $B_{\rm tag}$ FEI probability. After this, the average multiplicity is reduced to 1.06 for simulated signal samples and 1.13 for data, with negligible statistical uncertainty. Multiple candidates arise from the exchange of photons or tracks that are displaced from the IP, which are not vetoed in the rest of event. If multiple signal candidates remain, we select one at random.

The dominant background contributions arise from continuum $e^+e^- \to q\bar{q}$ processes and nonsignal $B\bar{B}$ decays. To suppress them, we use a boosted decision tree (BDT) [34]. The BDT uses 32 input variables: 26 variables related to kinematics, the rest of event, and event shape, selected for their separation power and good data-simulation agreement, and six variables specifically designed to suppress backgrounds from D mesons. The list of input variables is provided in Supplemental Material [35].

Among the 32 BDT-input variables, $E_{\rm extra}$ provides the largest signal-background discrimination. We require the BDT output, denoted $\mathcal{O}_{\rm BDT}$ and ranging from 0 to 1, to be greater than 0.86. This criterion is chosen to include the point that maximizes the figure of merit (FOM), defined as $N_{\rm sig}/\sqrt{N_{\rm sig}+N_{\rm bkg}}$, where $N_{\rm sig}$ and $N_{\rm bkg}$ are the expected numbers of signal and background events. According to the simulation, the $\mathcal{O}_{\rm BDT}$ requirement retains 68% of signal events while rejecting 97% of background. The expected background yield is 3338 events, comprising 1568 $q\bar{q}$ and 1770 $B\bar{B}$ events. This total includes 4.0 ± 0.9 events from the $B^+ \to \tau^+(\to X_s^+\bar{\nu})\nu$ background. In the simulated signal sample, the ratio of charged to neutral B decay modes is approximately 2.7:1.

A signal region is defined in $M_{X_s}^{\rm reco} \times \mathcal{O}_{\rm BDT}$ space and divided into 3×5 bins. The bin boundaries along the $M_{X_s}^{\rm reco}$ axis, $[0.0, 0.6, 1.0, 2.0]$ GeV/c^2, correspond to regions dominated by K, K^*, and higher-mass X_s states, labeled MR1, MR2, and MR3. The boundary between MR2 and MR3 is set to 1.0 GeV/c^2, slightly below the nonresonant generation threshold of 1.1 GeV/c^2, to minimize sensitivity to the modeling of the nonresonant X_s generation point. In MR1, MR2, and MR3, the bin boundaries along the $\mathcal{O}_{\rm BDT}$ axis are [0.86, 0.9195, 0.979, 0.986, 0.993, 1.0], [0.86, 0.8925, 0.925, 0.95, 0.975, 1.0], and [0.86, 0.9, 0.94, 0.96, 0.98, 1.0], respectively. These bin boundaries are chosen to maximize sensitivity without introducing fit bias, which is verified by a pseudoexperiment study. For simplicity, bin indices are assigned from 1 to 15. The indices range from 1 to 5 in MR1, from 6 to 10 in MR2, and from 11 to 15 in MR3, increasing along the positive $\mathcal{O}_{\rm BDT}$ axis within each mass region.

We perform a binned maximum likelihood fit to the $M_{X_s}^{\rm reco} \times \mathcal{O}_{\rm BDT}$ distribution to determine the signal yields in three $M_{X_s}^{\rm true}$ regions; $0.0 < M_{X_s}^{\rm true} < 0.6$ GeV/c^2, $0.6 \le M_{X_s}^{\rm true} < 1.0$ GeV/c^2 and 1.0 GeV/$c^2 \le M_{X_s}^{\rm true}$, where $M_{X_s}^{\rm true}$ is the true mass of the X_s system, obtained from the simulation. The relationship between reconstructed and true mass, including cross-feed between regions, is derived from the signal simulation. We use the HistFactory [42] package to construct the probability density function (PDF) as the product of Poisson distributions and auxiliary terms. The expected numbers of events for the Poisson distributions are determined from simulation and includes correction factors and systematic uncertainties, described below. We introduce nuisance parameters to the likelihood with Gaussian constraints and parametrize systematic uncertainties as auxiliary terms. The values of the nuisance parameters and the signal branching fractions are determined by the fit.

Data-driven corrections are applied to the modeling. The $B^+ \to K^+\nu\bar{\nu}$ analysis [7] observed a mismodeling of the photon multiplicity in Belle II. This mismodeling likely arises from beam-related backgrounds and energy deposits from hadrons. To address this, we compare the photon multiplicity distributions in data and simulation using $B_{\rm tag}^{\pm}X_s^0$ candidates formed by combining a charged $B_{\rm tag}$ candidate and a neutral X_s candidate. Correction factors are derived from the ratio of data to simulation. We reweight simulation samples as a function of the photon multiplicity to correct for the disagreement. The simulation of the fragmentation of the X_s system is corrected using results from a measurement of $B \to X_s\gamma$ [43] in three $M_{X_s}^{\rm true}$ regions: $[1.15, 1.5]$ GeV/c^2, $[1.5, 2.0]$ GeV/c^2, and $[2.0, 2.4]$ GeV/c^2. Corrections are applied to nine decay mode categories: $K\pi$ without π^0, $K\pi$ with one π^0, $K2\pi$ without π^0, $K2\pi$ with one π^0, $K3\pi$ without π^0, $K3\pi$ with one π^0, $K4\pi$ with at most one π^0, decay modes including

$2\pi^0$, and decay modes including $3K$. The $B \to X_s n\bar{n}$ and $B \to X_s K_L^0 K_L^0$ decays constitute peaking backgrounds and require accurate modeling. For the modeling of $B \to K^{(*)} n\bar{n}$ decays, branching fractions are corrected using measurements of $B \to K^{(*)} p\bar{p}$ decays [44–46], and the distribution of neutron-pair invariant mass, $M_{n\bar{n}}$, is modeled using the distribution of proton-pair mass, $M_{p\bar{p}}$, from these decays. To correct the remaining $B \to X_s n\bar{n}$ simulation samples, we reconstruct $B \to X_s p\bar{p}$ events in data and use the measured $M_{p\bar{p}}$ distribution to reweight the simulated $M_{n\bar{n}}$ shape. The kinematics and branching fractions of $B^+ \to K^+ K_L^0 K_L^0$ and $B^0 \to K_S^0 K_L^0 K_L^0$ are corrected based on the observed $B^+ \to K^+ K_S^0 K_S^0$ [47] and $B^0 \to K_S^0 K_S^0 K_S^0$ [48,49] distributions, respectively. The modeling of $B \to K^* K_L^0 K_L^0$ and the remaining $B \to X_s K_L^0 K_L^0$ decays is corrected using reconstructed $B \to K^* K_S^0 K_S^0$ and $B \to X_s K_S^0 K_S^0$ decays.

Four samples are used for corrections to and validation of the PDFs, and for estimating the PDF-related systematic uncertainties: the off-resonance data, an $M_{\rm bc}$ sideband, an $\mathcal{O}_{\rm BDT}$ sideband, and a $B \to J/\psi X_s$ sample. To estimate the systematic uncertainty for the $\mathcal{O}_{\rm BDT}$ distribution for $e^+e^- \to q\bar{q}$ background, a BDT with the same input variables is trained to distinguish off-resonance data from simulation [50]. A weight $\sqrt{t/(1-t)}$, where t is the BDT output, is applied to each event of the on-resonance $e^+e^- \to q\bar{q}$ simulation sample. The resulting $\mathcal{O}_{\rm BDT}$ distribution is used in the fit, and the changes in the signal branching fractions are taken as systematic uncertainties. Additionally, data-to-simulation efficiency ratios are measured to be 1.21 ± 0.13, 0.90 ± 0.20, and 0.78 ± 0.10 for MR1, MR2, and MR3, respectively. These ratios are applied as correction factors to the $q\bar{q}$ efficiencies, and their statistical uncertainties are assigned as systematic uncertainties. The $\mathcal{O}_{\rm BDT}$ distribution for $B\bar{B}$ events is validated with the $M_{\rm bc}$ sideband, defined as $5.20\ {\rm GeV}/c^2 < M_{\rm bc} < 5.26\ {\rm GeV}/c^2$, and with the $\mathcal{O}_{\rm BDT}$ sideband, defined as $0.80 < \mathcal{O}_{\rm BDT} < 0.86$. We compare the efficiencies of the $\mathcal{O}_{\rm BDT}$ requirement between data and simulation samples using $B \to J/\psi X_s$ events with $J/\psi \to \mu^+\mu^-$. The reconstruction and selection procedures are the same as for the $B \to X_s \nu\bar{\nu}$ analysis, except for the selection of a $J/\psi \to \mu^+\mu^-$ candidate. We require the invariant mass of the J/ψ candidate to be within $0.05\ {\rm GeV}/c^2$ of the nominal mass [33]. The B candidate from the $B \to J/\psi X_s$ decay must satisfy $M_{\rm bc} > 5.25\ {\rm GeV}/c^2$ and $|\Delta E| < 0.1$ GeV. The event is then treated as a $B \to X_s \nu\bar{\nu}$ event by ignoring the muons from $J/\psi \to \mu^+\mu^-$. We verified using simulation that the $\mathcal{O}_{\rm BDT}$ selection efficiencies are consistent between $B \to J/\psi X_s$ and signal decays for MR1 and MR2. The data-to-simulation $\mathcal{O}_{\rm BDT}$ selection efficiency ratios are 1.00 ± 0.04, 1.05 ± 0.08, and 0.97 ± 0.14 for MR1, MR2, and MR3, respectively. These ratios are used as correction factors, and their statistical uncertainties are assigned as systematic uncertainties.

TABLE I. Summary of the dominant systematic uncertainties and the total contribution from subdominant uncertainties on $\mathcal{B}(B \to X_s \nu\bar{\nu})$ in the entire $M_{X_s}^{\rm true}$ range. The impact on the branching fraction uncertainty $\sigma_{\mathcal{B}}$ from each source is estimated by fixing the corresponding nuisance parameter in the minimization procedure and subtracting its uncertainty in quadrature from the total uncertainty. Due to correlations among sources, the quadrature sum of individual uncertainties does not equal the total uncertainty.

Source	Impact on $\sigma_{\mathcal{B}}$ $[10^{-5}]$
Simulated-sample size	6.0
Background normalization	5.7
Branching fractions of major B-decays	2.3
Nonresonant $X_s\nu\bar{\nu}$ generation range	2.1
$\mathcal{O}_{\rm BDT}$ selection efficiency	2.1
Photon multiplicity correction	1.8
$q\bar{q}$ background efficiency	1.8
Other subdominant contributions	3.1
Total systematic sources	11.7

Table I shows a summary of the dominant systematic uncertainties. The finite size of the simulation samples used to determine the PDF shapes is included as a source of systematic uncertainty, and is dominated by the limited statistics of the background simulation samples. The ratio of data to simulation in the $M_{\rm bc}$ and $\mathcal{O}_{\rm BDT}$ sideband regions shows a maximum deviation of 12%. A conservative systematic uncertainty of $\pm 20\%$ is assigned to the background normalization in each $M_{X_s}^{\rm reco}$ region: MR1, MR2, and MR3. To estimate the systematic uncertainty of the photon multiplicity correction factor, we compare the photon multiplicity distributions in data and simulation with $B_{\rm tag}^0 X_s^{\pm}$ candidates. The residual difference is assigned as the systematic uncertainty of photon multiplicity correction factor. The lower bound on the $M_{X_s}^{\rm true}$ mass when generating the nonresonant $B \to X_s \nu\bar{\nu}$ component is set to $1.1\ {\rm GeV}/c^2$. We assign a systematic uncertainty of $\pm 0.1\ {\rm GeV}/c^2$ to this value, which is conservatively estimated from the $M_{X_s}^{\rm true}$ distribution of $B \to X_s\gamma$, $B^0 \to K^+\pi^-\mu^+\mu^-$, and $B^+ \to K^+\pi^+\pi^-\mu^+\mu^-$ decays [24–26]. The impact of an S-wave $K\pi$ component in the $M_{X_s}^{\rm true} < 1.0\ {\rm GeV}/c^2$ region was determined with simulation to have a negligible effect. The impact of varying the branching fractions of the leading B meson decays [33] is also included as a systematic uncertainty. The full list of contributions to the systematic uncertainty, including subdominant contributions, is included in Supplemental Material [35].

The postfit distribution of the bin index is shown in Fig. 2. The branching fractions, given in Table II, are calculated as $\mathcal{B} = N_{\rm sig}/(2 \times N_{BB} \times \epsilon)$, where N_{BB} is

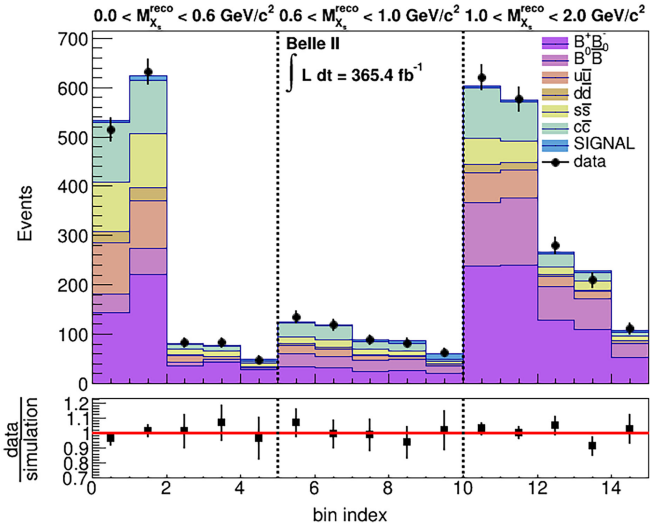


FIG. 2. The bin index distribution after the fit, for data and histogram templates. The background templates are separated into 6 categories: charged B meson decay, neutral B meson decay, and four types of $e^+e^- \to q\bar{q}$ background ($q = u, d, s, c$).

determined as in Ref. [51]. The signal distribution is shown separately in Supplemental Material [35]. The observed signal yields are not significant, and upper limits (ULs) on the branching fractions are determined using the CL_s method [52]. The CL_s values are shown in Supplemental Material [35]. The central value of $\mathcal{B}(B \to K\nu\bar{\nu})$ determined from the fit results is $[0.3 \pm 0.8(\text{stat})^{+0.8}_{-0.7}(\text{syst})] \times 10^{-5}$, consistent with the value $[1.1^{+0.9}_{-0.8}(\text{stat})^{+0.8}_{-0.5}(\text{syst})] \times 10^{-5}$ obtained in the dedicated $B^+ \to K^+\nu\bar{\nu}$ analysis [7].

After unveiling the signal region, which had not been examined during the optimization of the analysis, we identified and corrected an error in the single-candidate selection. This resulted in a 2.6% change in the mean upper limit expected from the simulation and a 0.6% change in the observed upper limit from data.

In summary, we search for $B \to X_s\nu\bar{\nu}$ decay using 365.4 fb^{-1} of $\Upsilon(4S)$ and 42.7 fb^{-1} of off-resonance data collected by the Belle II experiment. The analysis reconstructs one B meson in a hadronic decay mode and considers 30 exclusive channels in the reconstruction of the X_s system. No significant signal is observed, and we set 90% CL upper limits on the partial branching fractions of 2.2×10^{-5} for $0.0 < M_{X_s}^{\text{true}} < 0.6$ GeV/c^2, 9.3×10^{-5} for $0.6 < M_{X_s}^{\text{true}} < 1.0$ GeV/c^2, and 3.1×10^{-4} for $1.0\ \text{GeV}/c^2 < M_{X_s}^{\text{true}}$. We calculate the branching fraction for the entire $M_{X_s}^{\text{true}}$ region by summing the partial branching fractions to find

$$\mathcal{B}(B \to X_s\nu\bar{\nu}) = [8.8^{+8.5}_{-8.2}(\text{stat})^{+12.6}_{-10.7}(\text{syst})] \times 10^{-5},$$

and set a corresponding 90% CL upper limit,

$$\mathcal{B}(B \to X_s\nu\bar{\nu}) < 3.3 \times 10^{-4}.$$

TABLE II. Efficiencies (ϵ), signal yields (N_{sig}), and branching-fraction ($\mathcal{B}$) central values and upper limits, where the subscripts obs and exp indicate observed and expected values, respectively. The efficiencies are determined from the fit, since they depend on nuisance parameters. The expected upper limit is calculated from the background-only hypothesis. The first and second uncertainties are statistical and systematic, respectively.

			$\mathcal{B}$ [10^{-5}]		
$M_{X_s}^{\text{true}}$ [GeV/c^2]	ϵ [10^{-3}]	N_{sig}	Central value	UL_{obs}	UL_{exp}
[0, 0.6]	2.93	6^{+18+19}_{-17-16}	$0.3 \pm 0.8^{+0.8}_{-0.7}$	2.2	2.0
[0.6, 1.0]	1.32	36^{+27+31}_{-26-26}	$3.5^{+2.7+3.1}_{-2.5-2.6}$	9.3	6.4
[1.0, m_B]	0.63	25^{+45+63}_{-43-53}	$5.1^{+9.2+12.9}_{-8.8-11.0}$	30.9	27.3
Full range	0.97	66^{+64+95}_{-61-81}	$8.8^{+8.5+12.6}_{-8.2-10.7}$	32.7	24.2

This branching fraction and upper limit do not include the contribution from long-distance $B^+ \to \tau^+(\to X_s^+\bar{\nu})\nu$ decays. This is the first search for inclusive $B \to X_s\nu\bar{\nu}$ decays and can be used to constrain potential contributions from physics beyond the SM [11].

Acknowledgments—This work, based on data collected using the Belle II detector, which was built and commissioned prior to March 2019, was supported by Higher Education and Science Committee of the Republic of Armenia Grant No. 23LCG-1C011; Australian Research Council and Research Grants No. DP200101792, No. DP210101900, No. DP210102831, No. DE220100462, No. LE210100098, and No. LE230100085; Austrian Federal Ministry of Education, Science and Research, Austrian Science Fund (FWF) Grants DOI: 10.55776/P34529, DOI: 10.55776/J4731, DOI: 10.55776/J4625, DOI: 10.55776/M3153, and DOI: 10.55776/PAT1836324 and Horizon 2020 ERC Starting Grant No. 947006 "InterLeptons"; Natural Sciences and Engineering Research Council of Canada, Digital Research Alliance of Canada, and Canada Foundation for Innovation; National Key R&D Program of China under Contracts No. 2024YFA1610503 and No. 2024YFA1610504; National Natural Science Foundation of China and Research Grants No. 11575017, No. 11761141009, No. 11705209, No. 11975076, No. 12135005, No. 12150004, No. 12161141008, No. 12405099, No. 12475093, and No. 12175041 and Shandong Provincial Natural Science Foundation Project No. ZR2022JQ02; the Czech Science Foundation Grant No. 22-18469S, Regional funds of EU/MEYS: OPJAK FORTE CZ.02.01.01/00/22_008/0004632 and Charles University Grant Agency Project No. 246122; European Research Council, Seventh Framework PIEF-GA-2013-622527, Horizon 2020 ERC-Advanced Grants No. 267104 and No. 884719, Horizon 2020 ERC-Consolidator Grant No. 819127, Horizon 2020 Marie

Sklodowska-Curie Grant Agreement No. 700525 "NIOBE" and No. 101026516, and Horizon 2020 Marie Sklodowska-Curie RISE project JENNIFER2 Grant Agreement No. 822070 (European grants); L'Institut National de Physique Nucléaire et de Physique des Particules (IN2P3) du CNRS and L'Agence Nationale de la Recherche (ANR) under Grant No. ANR-23-CE31-0018 (France); BMFTR, DFG, HGF, MPG, and AvH Foundation (Germany); Department of Atomic Energy under Project Identification No. RTI 4002, Department of Science and Technology, and UPES SEED funding programs No. UPES/R&D-SEED-INFRA/17052023/01 and No. UPES/R&D-SOE/20062022/06 (India); Israel Science Foundation Grant No. 2476/17, U.S.-Israel Binational Science Foundation Grant No. 2016113, and Israel Ministry of Science Grant No. 3-16543; Istituto Nazionale di Fisica Nucleare and the Research Grants BELLE2, and the ICSC—Centro Nazionale di Ricerca in High Performance Computing, Big Data and Quantum Computing, funded by European Union—NextGenerationEU; Japan Society for the Promotion of Science, Grant-in-Aid for Scientific Research Grants No. 16H03968, No. 16H03993, No. 16H06492, No. 16K05323, No. 17H01133, No. 17H05405, No. 18K03621, No. 18H03710, No. 18H05226, No. 19H00682, No. 20H05850, No. 20H05858, No. 22H00144, No. 22K14056, No. 22K21347, No. 23H05433, No. 26220706, and No. 26400255, and the Ministry of Education, Culture, Sports, Science, and Technology (MEXT) of Japan; National Research Foundation (NRF) of Korea Grants No. 2021R1-F1A-1064008, No. 2022R1-A2C-1003993, No. 2022R1-A2C-1092335, No. RS-2016-NR017151, No. RS-2018-NR031074, No. RS-2021-NR060129, No. RS-2023-00208693, No. RS-2024-00354342 and No. RS-2025-02219521, Radiation Science Research Institute, Foreign Large-Size Research Facility Application Supporting project, the Global Science Experimental Data Hub Center, the Korea Institute of Science and Technology Information (K25L2M2C3) and KREONET/GLORIAD; Universiti Malaya RU grant, Akademi Sains Malaysia, and Ministry of Education Malaysia; Frontiers of Science Program Contracts No. FOINS-296, No. CB-221329, No. CB-236394, No. CB-254409, and No. CB-180023, and SEP-CINVESTAV Research Grant No. 237 (Mexico); the Polish Ministry of Science and Higher Education and the National Science Center; the Ministry of Science and Higher Education of the Russian Federation and the HSE University Basic Research Program, Moscow; University of Tabuk Research Grants No. S-0256-1438 and No. S-0280-1439 (Saudi Arabia), and Researchers Supporting Project number (RSPD2025R873), King Saud University, Riyadh, Saudi Arabia; Slovenian Research Agency and Research Grants No. J1-50010 and No. P1-0135; Ikerbasque, Basque Foundation for Science, State Agency for Research of the Spanish Ministry of Science and Innovation through Grant No. PID2022-136510NB-C33, Spain, Agencia Estatal de Investigacion, Spain Grant No. RYC2020-029875-I and Generalitat Valenciana, Spain Grant No. CIDEGENT/2018/020; The Knut and Alice Wallenberg Foundation (Sweden), Contracts No. 2021.0174, No. 2021.0299, and No. 2023.0315; National Science and Technology Council, and Ministry of Education (Taiwan); Thailand Center of Excellence in Physics; TUBITAK ULAKBIM (Turkey); National Research Foundation of Ukraine, Project No. 2020.02/0257, and Ministry of Education and Science of Ukraine; the U.S. National Science Foundation and Research Grants No. PHY-1913789 and No. PHY-2111604, and the U.S. Department of Energy and Research Awards No. DE-AC06-76RLO1830, No. DE-SC0007983, No. DE-SC0009824, No. DE-SC0009973, No. DE-SC0010007, No. DE-SC0010073, No. DE-SC0010118, No. DE-SC0010504, No. DE-SC0011784, No. DE-SC0012704, No. DE-SC0019230, No. DE-SC0021274, No. DE-SC0021616, No. DE-SC0022350, and No. DE-SC0023470; and the Vietnam Academy of Science and Technology (VAST) under Grants No. NVCC.05.02/25-25 and No. DL0000.05/26-27. These acknowledgements are not to be interpreted as an endorsement of any statement made by any of our institutes, funding agencies, governments, or their representatives. We thank the SuperKEKB team for delivering high-luminosity collisions; the KEK cryogenics group for the efficient operation of the detector solenoid magnet and IBBelle on site; the KEK Computer Research Center for on-site computing support; the NII for SINET6 network support; and the raw-data centers hosted by BNL, DESY, GridKa, IN2P3, INFN, and the University of Victoria.

Data availability—Numerical data corresponding to the results presented are available as HEPData [53]. The full Belle II data are not publicly available. The collaboration will consider requests for access to the data that support this article.

[1] S. L. Glashow, J. Iliopoulos, and L. Maiani, Weak interactions with lepton-hadron symmetry, Phys. Rev. D **2**, 1285 (1970).

[2] A. Khodjamirian, T. Mannel, A. A. Pivovarov, and Y. M. Wang, Charm-loop effect in $B \to K^{(*)}\ell^+\ell^-$ and $B \to K^*\gamma$, J. High Energy Phys. 09 (2010) 089.

[3] S. Sahoo, R. Mohanta, and A. K. Giri, Explaining the R_K and $R_{D^{(*)}}$ anomalies with vector leptoquarks, Phys. Rev. D **95**, 035027 (2017).

[4] A. J. Buras, F. De Fazio, and J. Girrbach, The Anatomy of Z' and Z with Flavour Changing Neutral Currents in the Flavour Precision Era, J. High Energy Phys. 02 (2013) 116.

[5] Z. Calcuttawala, A. Kundu, S. Nandi, and S. K. Patra, Optimal observable analysis for the decay $b \to s$ plus missing energy, Eur. Phys. J. C **77**, 650 (2017).

[6] A. J. Buras, J. Harz, and M. A. Mojahed, Disentangling new physics in $K \to \pi\nu\bar{\nu}$ and $B \to K(K^*)\nu\bar{\nu}$ observables, J. High Energy Phys. 10 (2024) 087.

[7] I. Adachi *et al.* (Belle II Collaboration), Evidence for $B^+ \to K^+\nu\bar{\nu}$ decays, Phys. Rev. D **109**, 112006 (2024).

[8] W. G. Parrott, C. Bouchard, and C. T. H. Davies (HPQCD Collaboration), Standard Model predictions for $B \to K\ell^+\ell^-$, $B \to K\ell_1^-\ell_2^+$ and $B \to K\nu\bar{\nu}$ using form factors from $N_f = 2 + 1 + 1$ lattice QCD, Phys. Rev. D **107**, 014511 (2023); **107**, 119903(E) (2023).

[9] M. Abumusabh *et al.* (Belle II Collaboration), Model-agnostic likelihood for the reinterpretation of the $B^+ \to K^+\nu\bar{\nu}$ measurement at Belle II, Phys. Rev. D **112**, 092016 (2025).

[10] A. J. Buras, J. Girrbach-Noe, C. Niehoff, and D. M. Straub, $B \to K^{(*)}\nu\bar{\nu}$ decays in the Standard Model and beyond, J. High Energy Phys. 02 (2015) 184.

[11] T. Felkl, S. L. Li, and M. A. Schmidt, A tale of invisibility: constraints on new physics in $b \to s\nu\nu$, J. High Energy Phys. 12 (2021) 118.

[12] R. Barate *et al.* (ALEPH Collaboration), Measurements of BR($b \to \tau^-\bar{\nu}_\tau X$) and BR($b \to \tau^-\bar{\nu}_\tau D^{*\pm} X$) and upper limits on BR($B^- \to \tau^-\bar{\nu}_\tau$) and BR($b \to s\nu\bar{\nu}$), Eur. Phys. J. C **19**, 213 (2001).

[13] T. Abe (Belle II Collaboration), Belle II technical design report, arXiv:1011.0352.

[14] K. Akai, K. Furukawa, and H. Koiso, SuperKEKB collider, Nucl. Instrum. Methods Phys. Res., Sect. A **907**, 188 (2018).

[15] T. Kuhr, C. Pulvermacher, M. Ritter, T. Hauth, and N. Braun (Belle II Framework Software Group), The Belle II Core Software, Comput. Softw. Big Sci. **3**, 1 (2019).

[16] Belle II Collaboration, Belle II Analysis Software Framework (BASF2), 10.5281/zenodo.5574115.

[17] D. J. Lange, The EvtGen particle decay simulation package, Nucl. Instrum. Methods Phys. Res., Sect. A **462**, 152 (2001).

[18] T. Sjöstrand, S. Ask, J. R. Christiansen, R. Corke, N. Desai, P. Ilten, S. Mrenna, S. Prestel, C. O. Rasmussen, and P. Z. Skands, An Introduction to PYTHIA 8.2, Comput. Phys. Commun. **191**, 159 (2015).

[19] S. Jadach, B. F. L. Ward, and Z. Wąs, The precision Monte Carlo event generator KK for two-fermion final states in e^+e^- collisions, Comput. Phys. Commun. **130**, 260 (2000).

[20] E. Barberio, B. van Eijk, and Z. Wąs, PHOTOS: A universal Monte Carlo for QED radiative corrections in decays, Comput. Phys. Commun. **66**, 115 (1991).

[21] S. Agostinelli *et al.* (Geant4 Collaboration), GEANT4: A simulation toolkit, Nucl. Instrum. Methods Phys. Res., Sect. A **506**, 250 (2003).

[22] W. G. Parrott, C. Bouchard, and C. T. H. Davies (HPQCD Collaboration), $B \to K$ and $D \to K$ form factors from fully relativistic lattice QCD, Phys. Rev. D **107**, 014510 (2023).

[23] A. Bharucha, D. M. Straub, and R. Zwicky, $B \to V\ell^+\ell^-$ in the Standard Model from light-cone sum rules, J. High Energy Phys. 08 (2016) 098.

[24] T. Saito *et al.* (Belle Collaboration), Measurement of the $\bar{B} \to X_s\gamma$ branching fraction with a sum of exclusive decays, Phys. Rev. D **91**, 052004 (2015).

[25] R. Aaij *et al.* (LHCb Collaboration), Measurements of the S-wave fraction in $B^0 \to K^+\pi^-\mu^+\mu^-$ decays and the $B^0 \to K^*(892)^0\mu^+\mu^-$ differential branching fraction, J. High Energy Phys. 11 (2016) 047; 04 (2017) 142(E).

[26] R. Aaij *et al.* (LHCb Collaboration), First observations of the rare decays $B^+ \to K^+\pi^+\pi^-\mu^+\mu^-$ and $B^+ \to \phi K^+\mu^+\mu^-$, J. High Energy Phys. 10 (2014) 064.

[27] A. Ali, G. Hiller, L. T. Handoko, and T. Morozumi, Power corrections in the decay rate and distributions in $B \to X_s\ell^+\ell^-$ in the Standard Model, Phys. Rev. D **55**, 4105 (1997).

[28] C. S. Kim, Y. G. Kim, and K. Y. Lee, Motion of a b quark inside a B meson: The parton model versus the Altarelli-Cabibbo-Corbo-Maiani-Martinelli model, Phys. Rev. D **57**, 4002 (1998).

[29] Y. Amhis *et al.* (Heavy Flavor Averaging Group), Averages of b-hadron, c-hadron, and τ-lepton properties as of 2021, Phys. Rev. D **107**, 052008 (2023).

[30] W. Altmannshofer, A. J. Buras, D. M. Straub, and M. Wick, New strategies for New Physics search in $B \to K^*\nu\bar{\nu}$, $B \to K\nu\bar{\nu}$ and $B \to X_s\nu\bar{\nu}$ decays, J. High Energy Phys. 04 (2009) 022.

[31] T. Keck *et al.*, The Full Event Interpretation, Comput. Softw. Big Sci. **3**, 6 (2019).

[32] J.-F. Krohn *et al.* (Belle II Analysis Software Group), Global decay chain vertex fitting at Belle II, Nucl. Instrum. Methods Phys. Res., Sect. A **976**, 164269 (2020).

[33] S. Navas *et al.* (Particle Data Group), Review of particle physics, Phys. Rev. D **110**, 030001 (2024).

[34] T. Keck, FastBDT: A speed-optimized multivariate classification algorithm for the Belle II experiment, Comput. Softw. Big Sci. **1**, 2 (2017).

[35] See Supplemental Material at http://link.aps.org/supplemental/10.1103/kf73-hw61 for details of the BDT input variables, systematic uncertainties, and supplementary figures, which includes Refs. [36–41].

[36] S. H. Lee *et al.* (Belle Collaboration), Evidence for $B^0 \to \pi^0\pi^0$, Phys. Rev. Lett. **91**, 261801 (2003).

[37] D. M. Asner *et al.* (CLEO Collaboration), Search for exclusive charmless hadronic B decays, Phys. Rev. D **53**, 1039 (1996).

[38] G. C. Fox and S. Wolfram, Event shapes in e^+e^- annihilation, Nucl. Phys. **B149**, 413 (1979); **B157**, 543(E) (1979).

[39] F. Abudinén *et al.* (Belle II Collaboration), A calibration of the Belle II hadronic tag-side reconstruction algorithm with $B \to X\ell\nu$ decays, arXiv:2008.06096.

[40] Y. Sato *et al.* (Belle Collaboration), Measurement of the lepton forward-backward asymmetry in $B \to X_s\ell^+\ell^-$ decays with a sum of exclusive modes, Phys. Rev. D **93**, 032008 (2016); **93**, 059901(A) (2016).

[41] A. Ali, P. Ball, L. T. Handoko, and G. Hiller, Comparative study of the decays $B \to (K, K^*)\ell^+\ell^-$ in the standard model and supersymmetric theories, Phys. Rev. D **61**, 074024 (2000).

[42] K. Cranmer, A. Shibata, W. Verkerke, L. Moneta, and G. H. Lewis, HistFactory: A tool for creating statistical models for use with RooFit and RooStats, CERN Report No. CERNOPEN-2012-016, 2012.

[43] S. Watanuki *et al.* (Belle Collaboration), Measurements of isospin asymmetry and difference of direct CP asymmetries

in inclusive $B \to X_s\gamma$ decays, Phys. Rev. D **99**, 032012 (2019).

[44] B. Aubert *et al.* (*BABAR* Collaboration), Evidence for the $B^0 \to p\bar{p}K^{*0}$ and $B^+ \to \eta_c K^{*+}$ decays and Study of the Decay Dynamics of B Meson Decays into $p\bar{p}h$ final states, Phys. Rev. D **76**, 092004 (2007).

[45] J. H. Chen *et al.* (Belle Collaboration), Observation of $B^0 \to p\bar{p}K^{*0}$ with a large K^{*0} polarization, Phys. Rev. Lett. **100**, 251801 (2008).

[46] J. T. Wei *et al.* (Belle Collaboration), Study of the decay mechanism for $B^+ \to p\bar{p}K^+$ and $B^+ \to p\bar{p}\pi^+$, Phys. Lett. B **659**, 80 (2008).

[47] J. P. Lees *et al.* (*BABAR* Collaboration), Study of CP violation in Dalitz-plot analyses of $B^0 \to K^+K^-K^0_S$, $B^+ \to K^+K^-K^+$, and $B^+ \to K^0_S K^0_S K^+$, Phys. Rev. D **85**, 112010 (2012).

[48] J. P. Lees *et al.* (*BABAR* Collaboration), Amplitude analysis and measurement of the time-dependent CP asymmetry of $B^0 \to K^0_S K^0_S K^0_S$ decays, Phys. Rev. D **85**, 054023 (2012).

[49] M. Gronau and J. L. Rosner, Symmetry relations in charmless $B \to PPP$ decays, Phys. Rev. D **72**, 094031 (2005).

[50] D. Martschei, M. Feindt, S. Honc, and J. Wagner-Kuhr, Advanced event reweighting using multivariate analysis, J. Phys. Conf. Ser. **368**, 012028 (2012).

[51] M. Abumusabh *et al.* (Belle and Belle II Collaborations), Observation of the decays $B^+ \to \Sigma_c(2455)^{++}\bar{\Xi}_c^-$ and $B^0 \to \Sigma_c(2455)^0\bar{\Xi}_c^0$, Phys. Rev. D **112**, L051101 (2025).

[52] A. L. Read, Presentation of search results: The CL_s technique, J. Phys. G **28**, 2693 (2002).

[53] Belle-II Collaboration, First search for $B \to X_s\nu\bar{\nu}$ decays, HEPData (collection), 10.17182/hepdata.169553 (2026).